# Highly Ordered Graphene Polydopamine Composite Allowing Fast Motion of Cations: Toward a High-Performance Microsupercapacitor

Adnane Bouzina, René Meng, Cyrille Bazin, Hubert Perrot, Ozlem Sel, Catherine Debiemme-Chouvy

# Highly ordered graphene polydopamine composite allowing fast motion of cations: toward a high-performance micro-supercapacitor

*Adnane Bouzina, René Meng, Cyrille Bazin, Hubert Perrot, Ozlem Sel*, Catherine Debiemme-Chouvy**

Dr. A. Bouzina, R. Meng, Dr. C. Bazin, Dr. H. Perrot, Dr. C. Debiemme-Chouvy
Sorbonne Université, CNRS, Laboratoire Interfaces et Systèmes Electrochimiques, LISE UMR 8235, 4 place Jussieu, F-75005 Paris, France
Email: catherine.debiemme-chouvy@sorbonne-universite.fr

Dr. O. Sel
Chimie du Solide et de l'Energie, UMR 8260, Collège de France, 11 Place Marcelin Berthelot, F-75231 Paris Cedex 05, France
Réseau sur le Stockage Electrochimique de l'Energie (RS2E), CNRS FR 3459, 33 Rue Saint Leu, F-80039 Amiens Cedex, France
Email: ozlem.sel@college-de-france.fr

**Keywords**
Graphene, polydopamine, composite, micro-supercapacitor, *ac*-electrogravimetry

**Abstract**

The simple and eco-friendly preparation of micro-supercapacitor still remains a great challenge. Here are presented the preparation and the characterizations of an all-solid symmetric micro-supercapacitor based on a new composite formed of highly ordered graphene sheets due to the presence of polydopamine between the layers which present a d-spacing of 0.356 nm. This graphene-polydopamine composite is prepared by electroreduction of graphene oxide (GO) followed by the electrooxidation of dopamine added into the initial solution, *i.e.*, after GO reduction. In $Na_2SO_4$ solution, this composite material shows excellent capacitance and stability even at high scan rate (2 $V \cdot s^{-1}$) and a very low relaxation time ($\tau_0$) of 62 ms. This value is in very good agreement with the high transfer kinetic and low transfer resistance values of the ions implied in the charge storage process ($Na^+ \cdot 2H_2O$ and $Na^+$) determined by *ac*-electrogravimetry. Finally, it is shown that the all-solid micro-supercapacitor (interdigitated electrodes obtained using a $CO_2$ laser and $Na_2SO_4$/PVA gel) prepared with this new composite delivers a remarkable energy density of 6.36 $mWh \cdot cm^{-3}$ for a power density of 0.22 $W \cdot cm^{-3}$ and exhibits an excellent cycling stability (98% of retention after 10,000 cycles at 2 $V \cdot s^{-1}$).

## 1. Introduction

Nowadays, miniaturized electrochemical capacitors, are attracting more and more interest in a variety of applications as alternative or complementary devices for electrolytic capacitors or micro-batteries because of their long lifetimes and fast charge/discharge capability. For example, in the biomedical domain and for sensor applications, micro-batteries suffer from regular replacement due to their short cycle life, this can lead to several economic and social issues, since this substitution process may require a surgical operation in the case of implantable biochips [1-4].

Based on active materials of the electrode and the charge storage mechanism, micro-supercapacitors (MSCs) can be classified into three categories. The first type is called electrochemical double-layer capacitors (EDLCs), they store energy by the formation of an electrostatic double layer created by the interaction between the ions of the electrolyte and the surface of the electrodes. The second one is pseudo-capacitors, which store energy through reversible surface redox reactions. The last one is a hybrid capacitor which consists of both EDLCs and pseudo-capacitors in a single device [5-6].

However, these power delivery systems suffer from the amount of energy they can store, especially at high discharge current densities, where the discharge time is lower than the relaxation time of the electrode (transition between pure capacitive and resistive behavior), due to the domination of the resistive component which dissipates energy *via* ohmic losses [7-8]. This remains a critical point for the integration of these MSCs in embedded microdevices [9]. That is to say that among all the desired properties of a micro-supercapacitor device, the high rate capability and more precisely the high frequency response is the most crucial property for their applications. Despite the fact that pseudo-capacitive materials show promising specific capacitances [10-13], their slow faradic redox reactions have a significant impact on their frequency response and consequently on their rate capabilities. Compared to pseudo-capacitive materials, EDLC electrodes show a relatively better characteristic frequency response (low time constant) due to their fast charge storage process (electro-adsorption/desorption) [7, 14].

Graphene-based materials have garnered significant attention as MSC electrodes in recent years. This is largely due to their exceptional properties, including a large specific surface area, low thickness, flexibility, and excellent electrical conductivity. These characteristics enable the rapid transport/transfer of electrolyte ions, making them ideal for ultrafast MSC devices [15-20]. For example, in a study reported by Wu *et al.* [18], a lithography technique was used to produce graphene based in-plane micro-supercapacitors. First, a thin film of graphene oxide (GO) was

deposited on the substrate by spin coating. Then, the GO film was reduced by using a $CH_4$-plasma treatment at 700 °C. After deposition of a gold interdigitated current collector by lithography, the part of the graphene layer not covered by the current collector was removed by oxygen plasma etching. This technique was then further developed to create graphene-polyaniline hybrid MSCs [21]. Liu *et al.* [22] fabricated a MSC using rGO-PEDOT/PSS film with a significant thickness of 58 µm and a small inter-electrode spacing of 100 µm ("gap" between the interdigital electrodes). The simplicity and speed of this technique were demonstrated by the preparation of 10 MSCs with different microelectrode sizes in 90 seconds. More recently, Yoon *et al.* [23] demonstrated the fabrication of laser-induced graphene (FsLIG) patterns on natural fallen leaves in ambient air using a UV femtosecond laser beam. The FsLIG microelectrodes formed on leaves showed lower sheet resistance than their synthetic polymer counterparts and exhibit an outstanding areal capacitance (34.7 $mF \cdot cm^{-2}$ at 5 $mV \cdot s^{-1}$) with an excellent cycling stability.

Herein, a graphene based composite electrode for micro-supercapacitor is reported. This composite is composed of electrochemically reduced graphene oxide (ERGO) and electrogenerated polydopamine (PDA), namely $ERGO_{PBS}$-PDA, and employed for the first time in all solid micro-supercapacitor devices. The resulting composite is highly ordered due to the presence of polydopamine between the graphene sheets. The composite electrode shows an ultra-fast frequency response ($\tau_0$) and a high rate capability, which greatly outperforms our previous work in terms of time constant and capacity retention, which was reported for an electrode with similar composition but showing significantly less structural order [4]. Thanks to the coupled electrogravimetric technic "*ac*-electrogravimetry", these outstanding properties are explained by the high transfer kinetics and low transfer resistance values of the species implied in the charge storage process. The properties of the composite were compared to the electrochemical reduced graphene oxide (ERGO) and to the compositeobtained in the presence of dopamine in the electrolyte used for the electroreduction of the graphene oxide ($ERGO_{PBS,DA}$-PDA) [8]. Finally, an all-solid micro-supercapacitor, prepared following an original process exhibits excellent properties.

## 2. Results and Discussion

### 2.1. ERGO$_{PBS}$-PDA composite: synthesis and characterizations

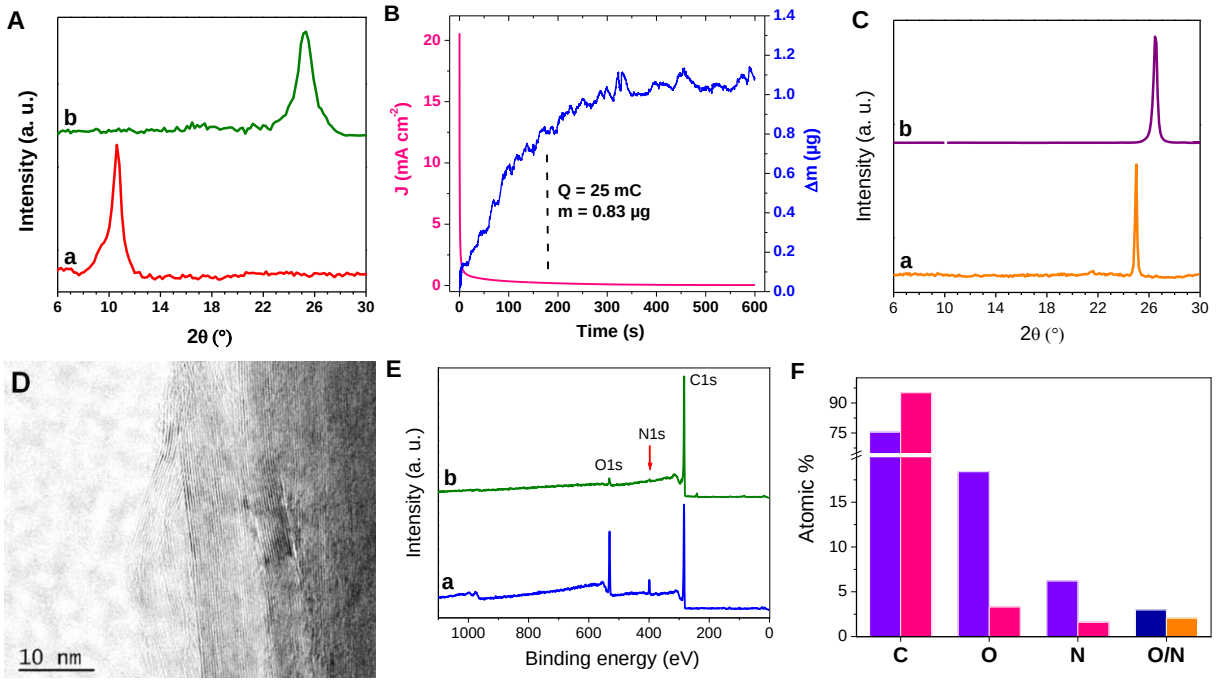


**Figure 1.** A) XRD diffractograms of a) pristine GO and b) ERGO$_{PBS}$ on Au/mica substrate. B) PDA electrodeposition on/in ERGO$_{PBS}$ in 5 mM DA + 0.2 M PBS (pH=7.2) solution. Current density (right axis) and electrode mass variation (left axis) as a function of the polarization time at 0.8 V *vs.* SCE. C) XRD diffractograms of a) ERGO$_{PBS}$-PDA and b) graphite. D) HR-TEM micrograph of ERGO$_{PBS}$-PDA. E) XPS survey spectra of ERGO$_{PBS}$-PDA a) before and b) after $Ar^+$ abrasion. F) Atomic % for C, O and N and ratio O/N determined by XPS of the ERGO$_{PBS}$-PDA composite before (blue) and after (pink, orange) ionic etching.

#### *2.1.1 GO electroreduction*

First, the GO film deposited on the electrode was electrochemically reduced in PBS solution called thereafter ERGO$_{PBS}$. **Figure 1A** shows the X-ray diffraction patterns of this ERGO film as well as the one of the pristine GO. Characteristic diffraction peak (001) of GO appeared at 2θ = 10.5° corresponding to a d-spacing of 0.842 nm, which is in good agreement with literature [8, 24-25]. After the electrochemical reduction of GO in the absence of dopamine (DA), ERGO$_{PBS}$, this peak (001) at 10.5 is no more detected, suggesting that the GO was fully reduced. Note that if dopamine molecules are present in the PBS solution a peak is still detected at 12.5° [8]. The difference observed between these two ERGO materials is obviously due to the

presence/absence of DA in the electrolyte used for the GO electroreduction. It is assumed that when dopamine molecules are present in the electrolyte, they interact with some oxygen-functional groups of the GO preventing their reduction.

After GO electroreduction a broad (002) peak emerged at 25.25° corresponding to an interlayer distance of 0.352 nm that is very consistent with the reported values, indicating a decrease of the space between the graphene sheets of the $ERGO_{PBS}$ film.[26]

### *2.1.2 Electrodeposition of PDA on/in the ERGO film*

After GO electroreduction, dopamine molecules were added to the electrolyte. EQCM measurements were performed to determine the simultaneous microbalance frequency changes, $\Delta f$, of the $ERGO_{PBS}$ modified quartz resonators during the electropolymerization of DA. **Figure 1B** shows the chronoamperogram and the electrode mass change due to the polydopamine deposition on/in the $ERGO_{PBS}$ film, as a consequence of the anodic oxidation of DA molecules. The electrode mass increases due to the formation of the PDA. The oxidation time of DA was optimized by checking the electrochemical response of the composite and the XRD diffractograms (**Figure S1** and **S2A**, respectively). From these results, it is obvious that 180 s of DA electrooxidation leads to the best characteristics. For this oxidation time, 0.83 µg of PDA was electrodeposited on/in the $ERGO_{PBS}$ coated quartz electrode (**Figure 1B**) whereas only 0.095 µg of PDA is electrodeposited on a blank Au-coated quartz electrode with the same surface as shown in reference [8]. This result confirms the presence of PDA between the graphene sheets for this composite, $ERGO_{PBS}$-PDA.

**Figure 1C-a** presents the XRD pattern of the $ERGO_{PBS}$-PDA composite film. Only one very sharp (narrow) peak located at 25.0° is observed, corresponding to a d-spacing of 0.356 nm. This finding indicates that the composite prepared by this new method (GO electroreduction in PBS followed by DA addition in the electrolyte and DA electroxidation) has a very high crystalline structure. Actually, this peak is as sharp as the one obtained for a graphite sample (**Figure 1C-b**). Thus, the electropolymerisation of DA added after GO electroreduction in PBS solution allows very well arranged graphene layers to be obtained, with a slight increase in the space between the sheets in comparison to the graphite *i.e.* 0.335 nm (**Figure 1C**). Thus, the presence of PDA into the ERGO leads on the one hand, to an increase of the space between the graphene layers (0.356 nm *versus* 0.335 nm) and on the other hand, to a very highly ordered graphene (narrow peak at 25.0° **Figure 1C-a**). To the best of our knowledge, it is the first time that a reduced graphene oxide is so well crystallized.

This finding was confirmed by TEM observations and XPS analyses. A TEM micrograph of the ERGO$_{PBS}$-PDA composite is presented in **Figure 1D**, it is clear that the graphene sheets are very well ordered. XPS analyses of the composite show the presence of N that can be attributed to the PDA (**Figure 1E** and **1F**). After an ionic etching of the composite surface, N is still detected, this result confirms that the PDA is not only at the film surface but also inside it. Moreover, after the ionic etching of the ERGO$_{PBS}$-PDA film that also leads to the removal of composite surface and of C and O contamination, the atomic ratio O/N, both atoms present in dopamine ($C_6H_3(OH)_2(CH_2)_2NH_3$), is 2.06 (**Figure 1F**), in very good agreement with the dopamine composition.

### 2.2. *Electrode/electrolyte interface processes investigated by EQCM and ac-electrogravimetry*

The ERGO$_{PBS}$-PDA composite was characterized by Electrochemical Quartz Crystal Microbalance (EQCM) and with advanced EQCM (*ac*-electrogravimetry) to investigate the electrochemical behavior, as well as the nature and kinetics of the species implied in the charge compensation process.

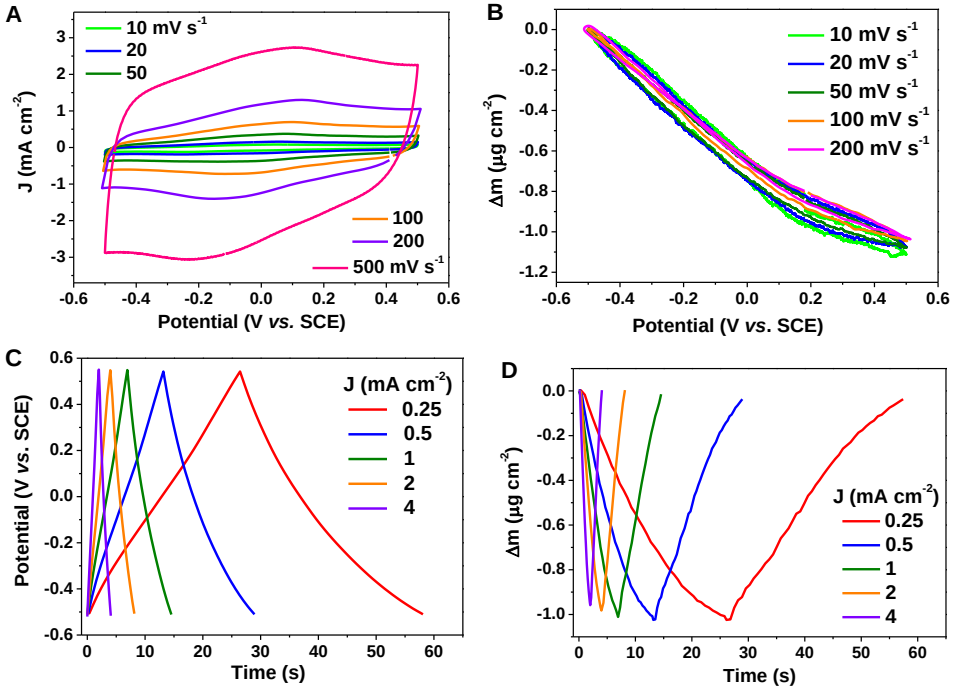


**Figure 2.** A) CV and B) mass change *vs*. applied potential of the ERGO$_{PBS}$-PDA composite at different potential scan rates. C, D) GCD and mass change *vs.* time, respectively, for various applied current densities.

### *2.2.1. EQCM response of the $ERGO_{PBS}$-PDA composite in 0.5 M $Na_2SO_4$*

The electrochemical properties of the $ERGO_{PBS}$-PDA composite electrode were first determined in a three-electrode configuration, using 0.5 M $Na_2SO_4$ solution as electrolyte. The cyclic voltammetry (CV) and the corresponding masse changes are presented in **Figure 2A** and **2B**, respectively. The CV curves show a quasi-rectangular shape, even at a relatively high scan rate of 500 $mV \cdot s^{-1}$, indicating the typical signature of EDLC. One can notice from **Figure S3A** that without PDA it is not the case. Moreover for the $ERGO_{PBS}$-PDA composite electrode small anodic and cathodic peaks are present too, they could be attributed to PDA. The EQCM response (**Figure 2B**) shows that during cathodic and anodic potential scans the mass of the electrode increases and decreases, respectively, no hysteresis is observed between the anodic and cathodic scans. This finding indicates that a major cationic contribution occurs in the charge balance process. Moreover, since the electrode mass variation in function of the applied potential is nearly independent of the potential scan rate (**Figure 2B**) for the $ERGO_{PBS}$-PDA composite electrode, unlike for the $ERGO_{PBS}$ electrode (**Figure S3B**), it can be concluded that the species transfers into the graphene sheets are the fastest in the composite.

From these EQCM measurements, the mass per electron (MPE), Fdm/dq, can be calculated. This parameter indicates the average molar mass of the ions participating in the charge compensation process within the electrodes. **Figure S4** presents the MPE of the $ERGO_{PBS}$-PDA calculated from the QCM-GCD response at 1 $mA \cdot cm^{-2}$, at the charge and at the discharge. It is found that the MPE varies between 40 and 15 $g \cdot mol^{-1}$ in the potential window studies in this work. This result indicates that charge compensation may involve more than one species. To have a more refined information in terms of the nature of the species and on their transfer kinetics, *ac*-electrogravimetry is employed.

### 2.2.2 *Ac*-electrogravimetry

In order to specify the species transfer (anion, cation, free water molecule) at the electrode/electrolyte interface of the ERGO and $ERGO_{PBS}$-PDA composite electrodes, *ac*-electrogravimetric studies, coupling EIS with the quartz crystal microbalance, were conducted in 0.5 M $Na_2SO_4$, at different potentials in the range of -0.5 to 0.5 V *vs*. SCE. Using this technique, two different transfer functions (TFs) can be obtained simultaneously, the first one is the classical EIS TF ($\frac{\Delta E}{\Delta I}(\omega)$) and the second one is the so-called electrogravimetric TF ($\frac{\Delta m}{\Delta E}(\omega)$) which reveals the variation of the mass of the electrode in response to the sinusoidal potential

perturbation (see SI). From the EIS TF, the charge/potential TF can be derived using the **Equation S1**.

**Figure 3A** and **3B** present the charge/potential TF, $\frac{\Delta q}{\Delta E}(\omega)$, of ERGO and ERGO$_{PBS}$-PDA composite, respectively, polarized at -0.3 V *vs.* SCE. This TF takes into account only the charged species involved in the charge balance process. For both electrodes, slightly suppressed loops of the charge/potential TF, $\frac{\Delta q}{\Delta E}(\omega)$, are observed which can be explained by the contribution of two or more ions having close transfer kinetics.

Unlike the charge/potential TF, $\frac{\Delta q}{\Delta E}(\omega)$, the electrogravimetric TF, $\frac{\Delta m}{\Delta I}(\omega)$, reveals the contribution of ions and non-charged species (solvent molecule) involving during the charge storage process.

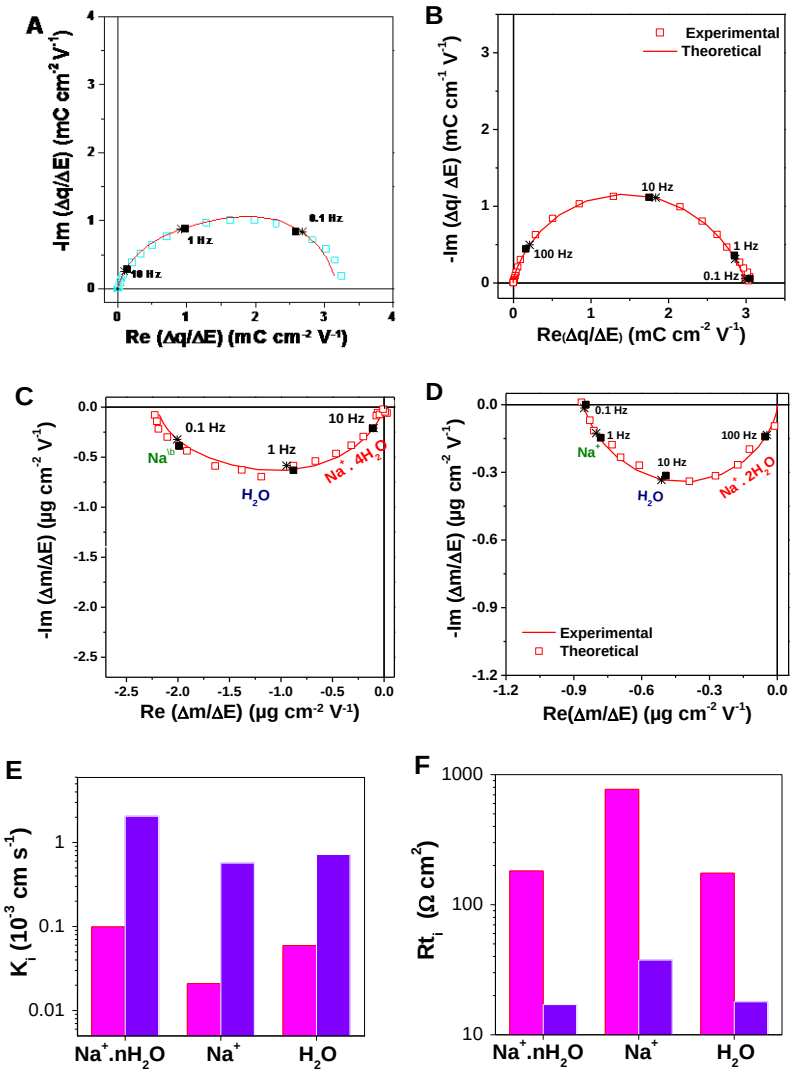


**Figure 3**. Experimental and theoretical *ac*-electrogravimetric data of (A, C) ERGO$_{PBS}$ and (B, D) ERGO$_{PBS}$-PDA at -0.3 V *vs.* SCE. (A, B) $\Delta q/\Delta E(\omega)$, (C, D) $\Delta m/\Delta E(\omega)$ transfer functions, in

0.5 M $Na_2SO_4$. E) $K_i$ and F) $Rt_i$ of ions and water molecule at -0.3 V/SCE, n=4 for $ERGO_{PBS}$ (pink), n=2 for $ERGO_{PBS}$-PDA (purple).

*Ac*-electrogravimetric experimental data were fitted by using the theoretical functions, **Equation S2** and **S3**. A good agreement of the experimental/theoretical curves was obtained, in terms of both shape and frequencies for both electrodes (see **Figure 3A** to **3D**). For $ERGO_{PBS}$ and $ERGO_{PBS}$-PDA, the fitting process revealed the implication of free water and two cationic species: hydrated sodium ($Na^+ \cdot 4H_2O$ for $ERGO_{PBS}$ and $Na^+ \cdot 2H_2O$ for $ERGO_{PBS}$-PDA) and bare $Na^+$.

The transfer kinetics of each species, $K_i$, obtained as a result of the fitting process are presented in **Figure 3E**. For both electrodes, hydrated cations exhibit the highest kinetics of transfer at the electrode/electrolyte interface, followed by $H_2O$ molecules. The free water molecules are probably electrodragged by the hydrated cations as they follow the same flow direction. This finding can be explained by the highly kosmotropic property of $Na^+$, which has a tendency to be adsorbed with a part of its hydration shell, as it was demonstrated by Levi *et al*. [27]. Although they are formally smaller than hydrated cations, dehydrated sodium cations were detected at low frequencies likely because their entire dehydration demands a higher amount of energy than partially dehydrated $Na^+$.

The transfer kinetics of the species in the case of $ERGO_{PBS}$-PDA are faster than in the case of $ERGO_{PBS}$. For example, the transfer of the hydrated cation is almost 20 times faster in $ERGO_{PBS}$-PDA than in $ERGO_{PBS}$ (**Figure 3E**). In other words, the $ERGO_{PBS}$-PDA composite exhibits excellent ion transfer capability in good agreement with the electrochemical response at high scan rate (**Figure 2A**). Notice that for the $ERGO_{PBS,DA}$-PDA composite the species are the same as for ERGO and the transfer kinetics, $K_i$, are between those obtained for ERGO and $ERGO_{PBS}$-PDA electrodes (see **Figure S6A, S7A** and **S7B**). In addition, $ERGO_{PBS}$-PDA composite exhibits low transfer resistance, $Rt_i$, compared to the ERGO electrode Over the entire range of the studied potentials (**Figure 3F, S6B** and **S7D**), which indicates an easier transfer of the active species into the $ERGO_{PBS}$-PDA material.

### *2.2.3. Comparison of EQCM and ac-electrogravimetric results*

To confirm our hypothesis deconvoluting the total mass response to charged species and free solvent molecule contributions to the charge storage process, a verification approach consisting

of the complementarity of the EQCM and *ac*-electrogravimetry was employed, following the procedure already described in literature.[28-31]

From *ac*-electrogravimetry, the relative concentration changes of exchanged species, $C_i - C_0$, as a function of the applied potential can be obtained. This quantity is estimated from the integration of the concentration/potential TF, $\frac{\Delta C}{\Delta E}(\omega)$, at low frequencies (**Equation S5**).

**Figure S8A** and **S9A** show the relative concentration changes ($C_i$ - $C_0$) of individual species in ERGO$_{PBS}$-PDA films and ERGO$_{PBS}$, respectively. For both electrodes, free water presents the highest concentration change in the potential range from -0.5 to 0.5 V *vs*. SCE, this phenomenon is often observed for carbon materials tested in aqueous electrolytes [1, 6-8] due maybe to the use of the strong kosmotropic nature of the electrolytic cations. Indeed, in a protic ionic liquid, pyrrolidinium hydrogen sulfate [Pyr$^+$][HSO$_4^-$], no water transfer was detected.[32] From the relative concentration changes ($C_i$ - $C_0$) values, the corresponding mass variations of each species can be obtained with consideration of their molar masses ($M_i$) (**Figure S8B** and **S9C**). The global mass response can be recalculated from *ac*-electrogravimetry by the addition of individual mass ($\Delta m_i$) of the three species detected by *ac*-electrogravimetry. From **Figures S8C and S9E**, it is clear that there is an excellent agreement between the reconstructed $\Delta m$ from the *ac*-electrogravimetry response and the EQCM mass response measured at a scan rate of 10 mV·s$^{-1}$. This finding validates the multi species exchange in charge-storage mechanism of the present systems and highlights the significant contribution of $H_2O$ molecules. Notice that same observation was done with the ERGO$_{PBS,DA}$-PDA composite (see **Figure S9F**) prepared in the presence of dopamine (DA) in the PBS solution in which GO is electroreduced.

### 2.3 Electrochemical performance in 3-electrode configuration

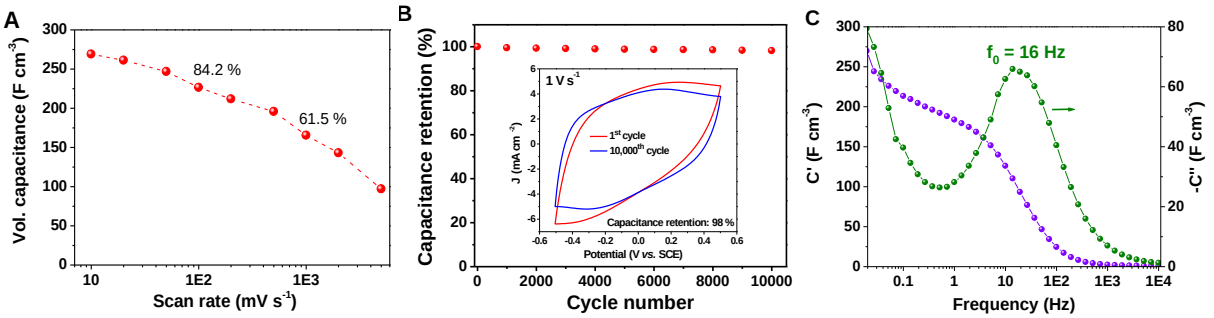


**Figure 4.** A) Volumetric capacitance of the ERGO$_{PBS}$-PDA film determined from CVs performed at different potential scan rates in 0.5 M $Na_2SO_4$. B) Capacitance retention of the ERGO$_{PBS}$-PDA film over 10000 cycles at scan rate 1 V·s$^{-1}$. Inset: CVs before and after 10,000

cycles. C) Bode plot of the volumetric capacitance of $ERGO_{PBS}$-PDA in the frequency range of 0.01 Hz to 10 kHz measured at −0.3 V vs SCE in 0.5 M $Na_2SO_4$.

With increasing the scan rate up to 1 $V \cdot s^{-1}$, $ERGO_{PBS}$-PDA composite still presents a high volumetric capacitance of 165 F $cm^{-3}$ (**Figure 4A**), indicating a better rate capability of the composite when GO is reduced in the absence of DA in the electrolyte [8]. This fast charge storage capability can be explained by the rapid ion transport pathways inside the $ERGO_{PBS}$-PDA material due to its well-ordered structure. This composite also demonstrates an excellent cycling stability with 98% of capacitance retention over 10,000 cycles at a scan rate of 1 $V \cdot s^{-1}$ as illustrated in **Figure 4B**.

For an EDLC electrode the capacitance is frequency dependent. It can be determined using EIS [33]. From the relationships between the real part of the complex capacitance, $C'(\omega)$, and the frequency shown in **Figure 4C**, it is found at low frequencies that the composite electrode has a capacitance of 274 $F \cdot cm^{-3}$. The Bode plot of imaginary part of the complex capacitance, $C''(\omega)$, of the $ERGO_{PBS}$-PDA exhibits a characteristic frequency ($f_0$) of 16 Hz at the maximal imaginary part of the capacitance, which corresponds to a characteristic time constant ($\tau_0 = 1/f_0$) of 0.065 s, much lower than the $\tau_0$ value obtained for $ERGO_{PBS,DA}$-PDA (0.88 s) [8], indicating the fast response and explaining the better rate capability of $ERGO_{PBS}$-PDA observed in the CV responses compared to $ERGO_{PBS,DA}$-PDA.

In comparison to some recent reports on carbon-based materials, the relaxation time of $ERGO_{PBS}$-PDA is smaller than the value obtained for multi-walled carbon nanotube (0.7 s), and for 3D graphene scaffold (0.53 s) [34]. The low value of $\tau_0$ corresponds to high power and is preferred for devices having rapid charging-discharging process. The value obtained for $ERGO_{PBS}$-PDA suggests that this electrode is able to deliver its stored energy at a much faster time at high power densities.

### 2.4 MSC preparation and characterizations

The promising results obtained in the three-electrode configuration of the $ERGO_{PBS}$-PDA composite have encouraged us to test this material as electrode material for all-solid-state interdigitated micro-supercapacitors. The all-solid micro-supercapacitor was prepared on a plexiglass substrate using a laser cutter following the steps shown in **Scheme 1.** Briefly, Ti/Au (10/100 nm) current collector was deposited by sputtering on a plexiglass substrate. Then, a GO

film was formed on the gold film by drop-casting 200 µL of a GO suspension (1 mg·mL$^{-1}$). Subsequently, a laser cutter was used to etch away some parts of the film to achieve the desired

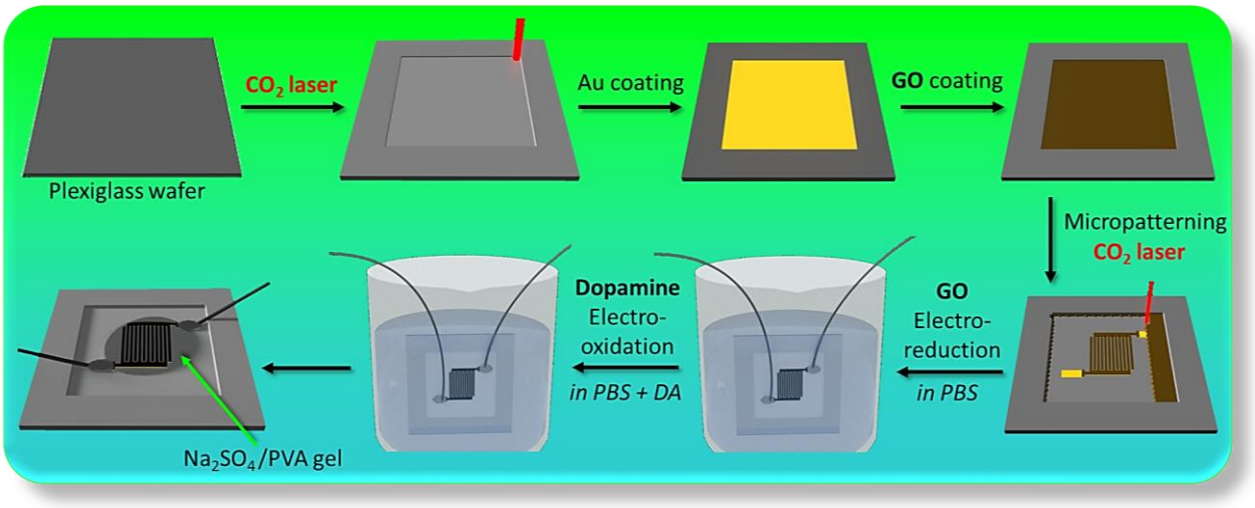


**Scheme 1.** Illustration of the preparation of the symmetric 2D MSC. The interdigitated electrodes are composed of electrochemically reduced graphene oxide-polydopamine composite obtained by an electrochemical way. PBS: phosphate buffered solution. DA: dopamine.

interdigitated pattern. After creating the interdigitated pattern, electrical wires were placed at the end of each electrode using silver paint for electrical contact and then insulated with silicone. The electrochemical reduction of GO deposited on the Au interdigitated electrodes and the electrodeposition of PDA were performed according to the conditions detailed previously in a conventional three-electrode cell, using the interdigitated (short-circuited) electrodes as the working electrode, a platinum grid and a saturated calomel electrode (SCE) as the counter and reference electrodes, respectively. Finally, a gel electrolyte based on $Na_2SO_4$/poly(vinyl alcohol) ($Na_2SO_4$/ PVA) was subsequently drop-cast onto the interdigitated microelectrodes and solidified overnight.

**Figure 5A** shows a digital photograph of the ERGO$_{PBS}$-PDA MSC formed on a plexiglass substrate. This MSC consists of 12 interdigital fingers (6 fingers per electrode). The width of the interdigital finger is about 500 µm (**Figure 5B**). The total area of these interdigital fingers is 0.75 cm$^2$. The inter-space between interdigital fingers was designed to be 200 µm (**Figure 5B**). It should be noted that no etching residue is observed in the inter-finger space, which ensures that there are no short-circuits in the microdevice (this was verified with an ohmmeter). A SEM micrograph of the cross-section of a finger is shown in **Figure 5C**. From this

micrograph one can conclude that the Au current collector is coated with a 600 nm thick ERGO$_{PBS}$-PDA film.

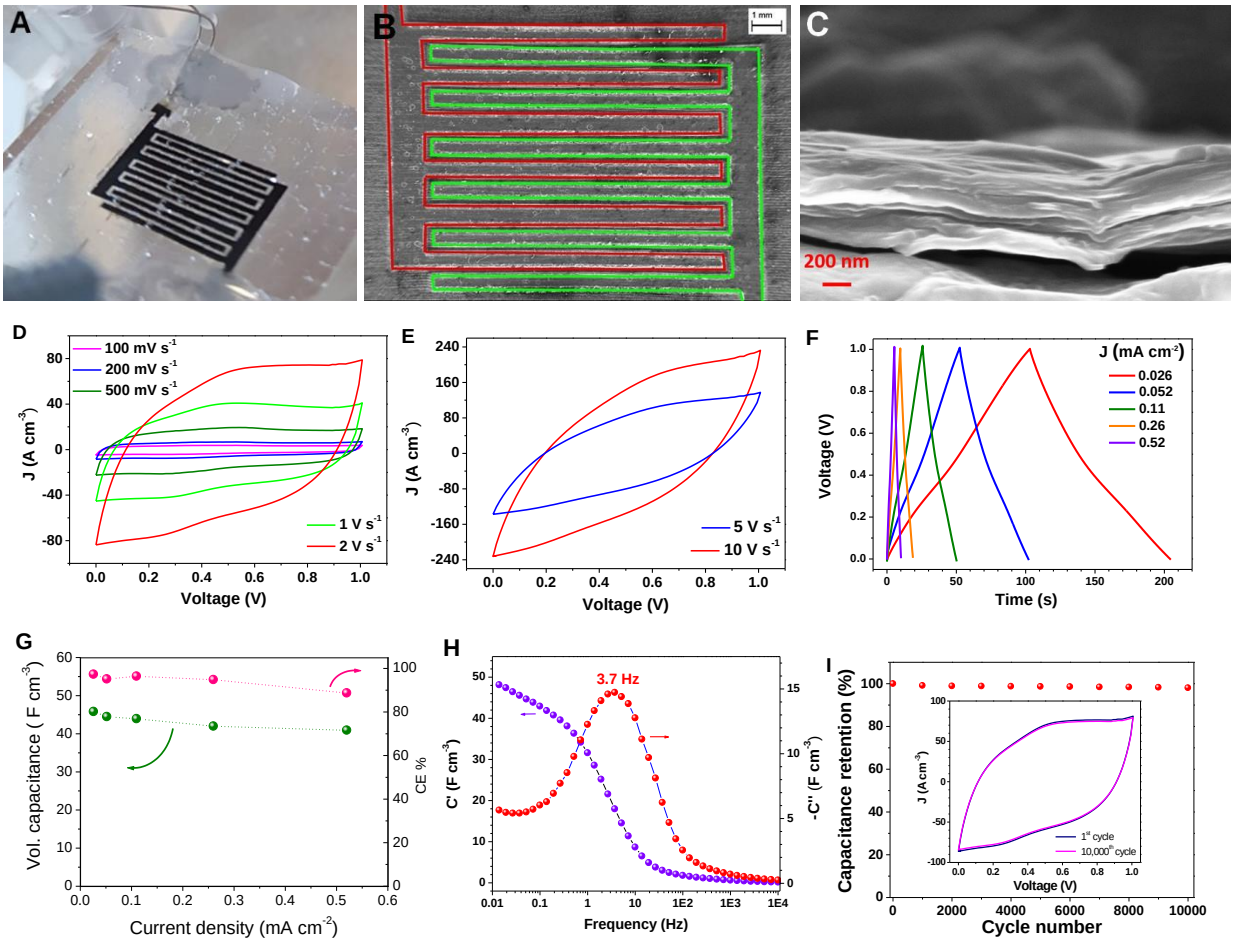


**Figure 5.** A) Digital photograph of the ERGO$_{PBS}$-PDA MSC on a Plexiglas substrate. B) SEM micrographs of the device (scale bar: 1 mm). C) SEM micrograph of the cross-section of an interdigitated ERGO$_{PBS}$-PDA finger. D,E) CV curves of ERGO$_{PBS}$-PDA MSC at different scan rates, from 0.1 V·s$^{-1}$ to 10 V·s$^{-1}$. F) GCD curves at different current densities. G) Volumetric capacitance of ERGO$_{PBS}$-PDA MSC determined from GCD curves and Coulombic efficiency as a function of the applied current density (right axis). H) Bode plot of the volumetric capacitance of ERGO$_{PBS}$-PDA MSC in the frequency range of 0.01 Hz to 10 kHz measured at 0.3 V. I) Capacitance retention of the ERGO$_{PBS}$-PDA MSC *vs*. cycle number. Inset: CVs before and after 10,000 cycles at 2 V·s$^{-1}$.

To evaluate the electrochemical performance of ERGO$_{PBS}$-PDA based MSC, cyclic voltammetry (CV) at different scan rates and galvanostatic charge/discharge measurements were performed. **Figure 5D** and **5E** show the CV curves of the as-prepared ERGO$_{PBS}$-PDA

MSC in the potential window of 0 to 1 V, at various scan rates from 0.1 to 10 $V \cdot s^{-1}$. The cyclic voltammograms of the $ERGO_{PBS}$-PDA based symmetric micro-device shows a quasi-rectangular shape in the voltage window of 0 and 1 V even at a high scan rate of 2 $V \cdot s^{-1}$. This indicates a fast charge-discharge kinetics of the MSC. Actually, as shown by **Figure S12** the MSC capacitance decreases only at very high scan rate (decrease of 62 % of the initial value at a scan rate of 5 $V.s^{-1}$).

**Figure 5F** shows the GCD curves of $ERGO_{PBS}$-PDA based MSC. The triangular signal, characteristic of supercapacitors, is observed for all the tested current densities. The calculated volumetric capacitance of the MSC from GCD curves with respect to different discharge currents is plotted in **Figure 5G**. As can be seen from this figure, the $ERGO_{PBS}$-PDA MSC exhibits a capacitance of 46 $F \cdot cm^{-3}$ (2.76 $mF \cdot cm^{-2}$) and a high coulombic efficiency of 97% at a current density of 0.026 $mA \cdot cm^{-2}$ (**Figure 5G**, right axis). Additionally, the $ERGO_{PBS}$-PDA MSC exhibits an excellent rate capability with capacitance retention of 92% and 89% of the initial value at 10-fold (0.26 $mA \cdot cm^{-2}$) and 20-fold (0.52 $mA \cdot cm^{-2}$) higher current densities, respectively. These features compare favorably to state-of-the-art of MSC performances based on graphene [35-36]. Such rate capability guarantees a promising power density of the as-prepared $ERGO_{PBS}$-PDA MSC under high operating rates.

The electrochemical capacitive behaviour of the $ERGO_{PBS}$-PDA MSC was further investigated by electrochemical impedance spectroscopy at a potential of 0.3 V over a frequency range from 10 mHz to 100 kHz. The Nyquist plot (**Figure S13A**) reveals a slope close to 90° in a high frequency range, indicating excellent capacitance characteristics. The equivalent series resistance (ESR, the intersection with x-axis at high-frequency) is about 8 $\Omega \cdot cm^2$. This resistance is mainly attributed to the electrical resistance of the electrode, as well as the electrolyte resistance [37]. The frequency response of the $ERGO_{PBS}$-PDA MSC was also studied. The evolution of the real part, $C'(\omega)$, and imaginary part, $C''(\omega)$, of the capacitance as a function of frequency are shown in **Figure 5H**. The maximum capacitance at low frequency, which corresponds to the real capacitance of the $ERGO_{PBS}$-PDA MSC, is close to 48 $F.cm^{-3}$. This result is in a good agreement with the capacitance values extracted from the galvanostatic charge-discharge curves at low current densities (**Figure 5F**). The imaginary capacitance $C''(\omega)$ exhibits a maximum at a characteristic frequency ($f_0$) of 3.7 Hz corresponding to a time constant ($\tau_0$) of 0.27 s, implying the efficient ion transport/electron conductance, which is much smaller than all-solid state graphene-based micro-supercapacitors (2.5 s) [38].

As a potential energy storage device, the long-term stability of MSCs should also be examined. The cycling performances of the $ERGO_{PBS}$-PDA MSC was further evaluated by the repeated CVs over 10,000 cycles at a scan rate of 2 $V.s^{-1}$. As shown in **Figure 5I**, a capacitance retention of 98% was obtained after 10,000 cycles, demonstrating the good cycling stability of the $ERGO_{PBS}$-PDA MSC. Impedance spectroscopy results recorded before and after 10,000 cycles at 2 $V{\cdot}s^{-1}$ (**Figure S13B**) show a slight increase in the charge transfer resistance of $ERGO_{PBS}$-PDA MSC with conservation of the linear part at low frequencies, which is consistent with the good capacitance retention.

The Ragone plot in **Figure S14** lists the volumetric energy/power densities of the $ERGO_{NoDA}$-PDA MSC, calculated based on the GCD profiles. The $ERGO_{NoDA}$-PDA MSC can deliver a volumetric energy density of 6.36 $mWh.cm^{-3}$ at a power density of 0.22 $W.cm^{-3}$. Even at a power density of 4.33 $W.cm^{-3}$, this MSC can still deliver an energy density of 5.73 $mWh.cm^{-3}$. Which exceeds the performance of all-solid MSCs based on carbon materials, recently reported in the literature [39-41]. Compared to MSCs based on other classes of materials such as MXene [42], our MSC exhibits comparable energy densities.

## 3. Conclusion

In summary, an innovative electrochemical approach was developed to fabricate a composite electrode based on ERGO and PDA, leading to a preeminently well-ordered graphene structure due to the presence of polydopamine between the graphene sheets as evidenced by XPS and XRD analyses. The optimized $ERGO_{PBS}$-PDA composite electrode presents high ultra-fast frequency response ($\tau_0$) and the high rate capability. Which is explained thanks to the *ac*-electrogravimetry studies by the high transfer kinetics and the low transfer resistance values of the species implied in the charge storage process. The performances of this composite in the three-electrode configuration encouraged us to fabricate $ERGO_{PBS}$-PDA based symmetrical all-solid-state interdigitated MSC using a laser cutter. The MSC based on $ERGO_{PBS}$-PDA exhibited an excellent rate capability and cycling stability (98% of retention after 10,000 cycles at 2 $V{\cdot}s^{-1}$) and delivered a remarkable energy density of 6.36 $mWh{\cdot}cm^{-3}$ for a power density of 0.22 $W{\cdot}cm^{-3}$, which is comparable or outperforms the most of the recently reported MSCs based on graphene or other classes of materials.

## 4. Experimental Section

***Materials:*** Dopamine (DA) hydrochloride, potassium phosphate monobasic ($KH_2PO_4$), potassium phosphate dibasic ($K_2HPO_4$) and sodium sulfate ($Na_2SO_4$) were purchased from Sigma Aldrich and used without further purification. GO suspension (4 $mg \cdot mL^{-1}$, dispersion in $H_2O$) was purchased from Sigma Aldrich and diluted with water to 1 $mg \cdot mL^{-1}$ of GO. Double distilled water (18.2 $M\Omega \cdot cm$, Purelab flex ELGA, water purification system) was employed for all solution preparations. Phosphate buffered saline solution (PBS) of pH 7.2 was obtained by mixing 0.1 M of $KH_2PO_4$ and 0.1 M of $K_2HPO_4$.

***Synthesis of $ERGO_{PBS}$-PDA Electrode:*** For $ERGO_{PBS}$ and $ERGO_{PBS}$-PDA composite preparation, 6 µL of the GO suspension were deposited onto the Au electrode and dried in air (film thickness: 200 nm), then GO was electroreduced under an applied potential of -1 V *vs.* SCE for 10 min (unless otherwise stated) in a solution of 0.2 M PBS (pH 7.2). In a consecutive step, dopamine at a concentration of 0.5 $mg \cdot mL^{-1}$ was added to the PBS solution and PDA was electrogenerated at 0.8 V *vs.* SCE for 180 s (unless otherwise stated). It is important to notice that the DA molecules were added in the PBS solution only after the electroreduction of GO and that the ERGO film was kept in the electrolyte, not dried.

***Electrochemical and Electrogravimetric Characterizations:*** The electrochemical and electrogravimetric characterizations were carried out using a standard three electrode configuration with an Autolab potentiostat (Metrohm, France). GO-coated gold (Au) electrode of quartz (S = 0.2 $cm^{-2}$) (AWS-Sensors, Spain) was used as the initial working electrode, a platinum grid and a saturated calomel electrode (SCE) were used as counter electrode and reference electrode, respectively.

For the classical EQCM analysis, a lab-made QCM coupled with an Autolab potentiostat (PGSTAT12) was used. Under the gravimetric regime, the mass variation, $\Delta m$, was obtained from $\Delta f$ by using of the Sauerbrey equation, $\Delta f = -k_s \times \Delta m$, where $k_s$ is the experimental mass sensitivity constant which has a value of 16.3 $Hz \cdot cm^2 \cdot g^{-1}$ for 9 MHz AT-cut QCM [43].

For *ac*-electrogravimetry measurements[44], a four-channel frequency response analyzer (FRA, Solartron 1254) and a lab-built potentiostat were used. The modified quartz electrode was polarized at selected potentials and a sinusoidal small amplitude potential perturbation (50 mV) was applied. The frequency range of the measurements was between 63 kHz and 10 mHz. The mass change, $\Delta m$, of the working electrode was measured simultaneously with the *ac* response, $\Delta I$, of the electrochemical system.

***Morphological and Compositional Characterizations:*** SEM observations were observed under a field emission gun scanning electron microscope (FEG−SEM) (Ultra55, Zeiss) operating at 5 kV. The HRTEM micrographs were obtained using a JEOL 2010 microscope (JEOL Ltd, Tokyo, Japan). XPS analyses were performed using an Omicron Argus X-ray photoelectron spectrometer with monochromatized Al Kα excitation (1486.6 eV) with band-pass energies of 100 and 20 eV for acquisition of the survey and high-resolution spectra, respectively. The XPS peak areas were determined after subtraction of a background using Shirley's method. Element peak intensities were corrected by the Scofield factors. All spectrum processing was carried out using Casa XPS software (Casa Software Ltd., UK). For the XPS analyses, the films were prepared on a gold-coated mica substrate. XRD was performed using a Philips PANalytical X'Pert Pro diffractometer with Cu Kα radiation (λ = 1.54184 Å). The samples were prepared on a glass substrate.

***Preparation of the $ERGO_{PBS}$-PDA MSC:*** The synthesis method of the micro-supercapacitor using $ERGO_{PBS}$-PDA as the electrode material is shown in **Figure 5**. This MSC was prepared on a Plexiglass substrate. First, a 2 cm square was etched on the substrate (Plexiglass) using a laser cutter (Trotec SP500, $CO_2$ laser), then a 100 nm gold (Au) layer (further used as current collector) was deposited by sputtering. A titanium sub-layer (10 nm) was intercalated between Plexiglass and the gold because of the poor adhesion of the gold on Plexiglass. Then, a GO film was deposited on the gold by drop-casting of 200 µL of a GO suspension (1 $mg \cdot mL^{-1}$). Finally, using the $CO_2$ laser, the undesired material areas (interdigitated finger spacing) were removed according to a pattern that was prepared through the software Trotec JobControl®. The laser power, scan rate and pulse duration were set to 35 W and 35 $cm \cdot s^{-1}$ and 1.25 ms, respectively.

***Preparation of the $Na_2SO_4$/PVA gel electrolyte:*** The $Na_2SO_4$/PVA gel electrolyte was prepared by adding 0.25 g of $Na_2SO_4$ and 0.25 g of PVA into 2.5 mL of distilled water and heated to 80 °C under vigorous stirring until the solution turned transparent. $Na_2SO_4$/PVA gel electrolyte was subsequently drop-cast onto the interdigitated patterns and solidified overnight.

***Electrochemical characterizations of the all-solid-state device:*** CV, GCD, and EIS were carried out using an Autolab potentiostat, at room temperature. CV was performed at different scan rates between 0.1 and 10 $V \cdot s^{-1}$ in the 0 - 1 V range. GCD was performed at current densities of 0.026–0.52 $mA \cdot cm^{-2}$. EIS spectra were recorded at a potential of 0.3 V in the frequency range of 0.01 Hz – 100 kHz with an amplitude of 10 mV.

## Supporting Information

Supporting Information is available from the Wiley Online Library or from the author.

## Acknowledgements

The authors thank the doctoral school, "Chimie Physique et Chimie Analytique de Paris-Centre" ED388 of Sorbonne University and the French Ministry of Education Scholarship.

The authors thank Sandra Casale from Sorbonne University for the HRTEM observations, and thank the FabLab of Sorbonne University (Paris, France).

## References

1. Bu, F.; Zhou, W. W.; Xu, Y. H.; Du, Y.; Guan, C.; Huang, W., Recent developments of advanced micro-supercapacitors: design, fabrication and applications. *Npj Flexible Electronics* **2020,** *4*, 31.
2. Liu, N. S.; Gao, Y. H., Recent Progress in Micro-Supercapacitors with In-Plane Interdigital Electrode Architecture. *Small* **2017,** *13,* 1701989.
3. Wang, J. H.; Li, F.; Zhu, F.; Schmidt, O. G., Recent Progress in Micro-Supercapacitor Design, Integration, and Functionalization. *Small Methods* **2019,** *3*, 1800367.
4. Yuan, S.; Fan, W.; Jin, Y.; Wang, D.; Liu, T., Free-standing flexible graphene-based aerogel film with high energy density as an electrode for supercapacitors. *Nano Materials Science* **2021,** *3* , 68.
5. Simon, P.; Gogotsi, Y., Materials for electrochemical capacitors. *Nature Materials* **2008,** *7*, 845.
6. Majumdar, D.; Maiyalagan, T.; Jiang, Z. Q., Recent Progress in Ruthenium Oxide-Based Composites for Supercapacitor Applications. *Chemelectrochem* **2019,** *6*, 4343.
7. Ye, J. L.; Wu, Y. C.; Xu, K.; Ni, K.; Shu, N.; Taberna, P. L.; Zhu, Y. W.; Simon, P., Charge Storage Mechanisms of Single-Layer Graphene in Ionic Liquid. *Journal of the American Chemical Society* **2019,** *141*, 16559.
8. Bouzina, A.; Perrot, H.; Sel, O.; Debiemme-Chouvy, C., Preventing Graphene from Restacking via Bioinspired Chemical Inserts: Toward a Superior 2D Micro-supercapacitor Electrode. *Acs Applied Nano Materials* **2021,** *4*, 4964.
9. Beidaghi, M.; Wang, C. L., Micro-Supercapacitors Based on Interdigital Electrodes of Reduced Graphene Oxide and Carbon Nanotube Composites with Ultrahigh Power Handling Performance. *Advanced Functional Materials* **2012,** *22*, 4501.
10. Jang, G. S.; Ameen, S.; Akhtar, M. S.; Shin, H. S., Cobalt oxide nanocubes as electrode material for the performance evaluation of electrochemical supercapacitor. *Ceramics International* **2018,** *44*, 588.
11. Wu, D.; Xie, X. B.; Zhang, Y. P.; Zhang, D. M.; Du, W.; Zhang, X. Y.; Wang, B., MnO2/Carbon Composites for Supercapacitor: Synthesis and Electrochemical Performance. *Frontiers in Materials* **2020,** *7,* 2.
12. Yu, Z. N.; Duong, B.; Abbitt, D.; Thomas, J., Highly Ordered MnO2 Nanopillars for Enhanced Supercapacitor Performance. *Advanced Materials* **2013,** *25*, 3302.
13. Zhang, X.; Zhang, R. J.; Xiang, C. L.; Liu, Y.; Zou, Y. J.; Chu, H. L.; Qiu, S. J.; Xu, F.; Sun, L. X., Polydopamine-assisted formation of Co3O4-nanocube-anchored reduced graphene oxide composite for high-performance supercapacitors. *Ceramics International* **2019,** *45*, 13894.

14. Mehare, M. D.; Deshmukh, A. D.; Dhoble, S. J., Bio-waste lemon peel derived carbon based electrode in perspect of supercapacitor. *Journal of Materials Science-Materials in Electronics* **2021,** *32*, 14057.
15. Zhao, X.; He, D.; You, B., Laser engraving and punching of graphene films as flexible all-solid-state planar micro-supercapacitor electrodes. *Materials Today Sustainability* **2022,** *17*, 100096.
16. Song, Z.; Miao, L.; Ruhlmann, L.; Lv, Y.; Zhu, D.; Li, L.; Gan, L.; Liu, M., Self-Assembled Carbon Superstructures Achieving Ultra-Stable and Fast Proton-Coupled Charge Storage Kinetics. *Advanced Materials* **2021,** *33*, 2104148.
17. Li, Y.; Park, T.; Kim, M.; Xie, H.; Yi, J. W.; Li, J.; Alshehri, S. M.; Ahamad, T.; Na, J.; Yamauchi, Y., Electrophoretic Deposition of Binder-Free MOF-Derived Carbon Films for High-Performance Microsupercapacitors. *Chemistry – A European Journal* **2020,** *26*, 10283.
18. Wu, Z. S.; Parvez, K.; Feng, X.; Müllen, K., Graphene-based in-plane micro-supercapacitors with high power and energy densities. *Nature Communications* **2013,** *4*, 2487.
19. Li, F.; Qu, J.; Li, Y.; Wang, J.; Zhu, M.; Liu, L.; Ge, J.; Duan, S.; Li, T.; Bandari, V. K.; Huang, M.; Zhu, F.; Schmidt, O. G., Stamping Fabrication of Flexible Planar Micro-Supercapacitors Using Porous Graphene Inks. *Advanced Science* **2020,** *7*, 2001561.
20. Jiang, Y.; Guo, F.; Liu, Y.; Xu, Z.; Gao, C., Three-dimensional printing of graphene-based materials for energy storage and conversion. *SusMat* **2021,** *1*, 304.
21. Wu, Z.-S.; Parvez, K.; Li, S.; Yang, S.; Liu, Z.; Liu, S.; Feng, X.; Müllen, K., Alternating Stacked Graphene-Conducting Polymer Compact Films with Ultrahigh Areal and Volumetric Capacitances for High-Energy Micro-Supercapacitors. *Advanced Materials* **2015,** *27*, 4054.
22. Liu, Y.; Weng, B.; Xu, Q.; Hou, Y.; Zhao, C.; Beirne, S.; Shu, K.; Jalili, R.; Wallace, G. G.; Razal, J. M.; Chen, J., Facile Fabrication of Flexible Microsupercapacitor with High Energy Density. *Advanced Materials Technologies* **2016,** *1*, 1600166.
23. Le, T.-S. D.; Lee, Y. A.; Nam, H. K.; Jang, K. Y.; Yang, D.; Kim, B.; Yim, K.; Kim, S.-W.; Yoon, H.; Kim, Y.-J., Green Flexible Graphene–Inorganic-Hybrid Micro-Supercapacitors Made of Fallen Leaves Enabled by Ultrafast Laser Pulses. *Advanced Functional Materials* **2022,** *32*, 2107768.
24. Lesiak, B.; Trykowski, G.; Toth, J.; Biniak, S.; Kover, L.; Rangam, N.; Malolepszy, A.; Stobinski, L., Effect of Microwave Treatment in a High Pressure Microwave Reactor on Graphene Oxide Reduction Process-TEM, XRD, Raman, IR and Surface Electron Spectroscopic Studies. *Materials* **2021,** *14,* 5728.
25. Shao, Y. Y.; Wang, J.; Engelhard, M.; Wang, C. M.; Lin, Y. H., Facile and controllable electrochemical reduction of graphene oxide and its applications. *Journal of Materials Chemistry* **2010,** *20*, 743.
26. Banda, H.; Aradilla, D.; Benayad, A.; Chenavier, Y.; Daffos, B.; Dubois, L.; Duclairoir, F., One-step synthesis of highly reduced graphene hydrogels for high power supercapacitor applications. *Journal of Power Sources* **2017,** *360*, 538.
27. Levi, M. D.; Sigalov, S.; Salitra, G.; Elazari, R.; Aurbach, D., Assessing the Solvation Numbers of Electrolytic Ions Confined in Carbon Nanopores under Dynamic Charging Conditions. *Journal of Physical Chemistry Letters* **2011,** *2*, 120.
28. Goubaa, H.; Escobar-Teran, F.; Ressam, I.; Gao, W.; El Kadib, A.; Lucas, I. T.; Raihane, M.; Lahcini, M.; Perrot, H.; Sel, O., Dynamic Resolution of Ion Transfer in Electrochemically Reduced Graphene Oxides Revealed by Electrogravimetric Impedance. *Journal of Physical Chemistry C* **2017,** *121*, 9370.
29. Gao, W. L.; Krins, N.; Laberty-Robert, C.; Perrot, H.; Sel, O., Scrutiny of the LiCoO2 Composite Electrode/Electrolyte Interface by Advanced Electrogravimetry and Implications for Aqueous Li-Ion Batteries. *Journal of Physical Chemistry C* **2021,** *125*, 3859.
30. Escobar-Teran, F.; Perrot, H.; Sel, O., Ion Dynamics at the Carbon Electrode/Electrolyte Interface: Influence of Carbon Nanotubes Types. *Materials* **2022,** *15,* 1867.
31. Halim, E.; Demir-Cakan, R.; Perrot, H.; El Rhazi, M.; Sel, O., Interfacial charge storage mechanisms of composite electrodes based on poly(ortho-phenylenediamine)/carbon nanotubes via advanced electrogravimetry. *Journal of Chemical Physics* **2022,** *156*, 124703.

32. Bouzina, A.; Perrot, H.; Debiemme-Chouvy, C.; Sel, O., Interface Properties of 2D Graphene-Polydopamine Composite Electrodes in Protic Ionic Liquid-Based Electrolytes Explored by Advanced Electrogravimetry. *Acs Applied Energy Materials* **2022,** 5, 14934.
33. Taberna, P. L.; Simon, P.; Fauvarque, J. F., Electrochemical characteristics and impedance spectroscopy studies of carbon-carbon supercapacitors. *Journal of the Electrochemical Society* **2003,** *150*, A292.
34. Zhai, T.; Lu, X. H.; Wang, H. Y.; Wang, G. M.; Mathis, T.; Liu, T. Y.; Li, C.; Tong, Y. X.; Li, Y., An Electrochemical Capacitor with Applicable Energy Density of 7.4 Wh/kg at Average Power Density of 3000 W/kg. *Nano Letters* **2015,** *15*, 3189.
35. Wu, M.; Li, Y.; Yao, B.; Chen, J.; Li, C.; Shi, G., A high-performance current collector-free flexible in-plane micro-supercapacitor based on a highly conductive reduced graphene oxide film. *Journal of Materials Chemistry A* **2016,** *4*, 16213.
36. Pei, Z.; Hu, H.; Liang, G.; Ye, C., Carbon-Based Flexible and All-Solid-State Micro-supercapacitors Fabricated by Inkjet Printing with Enhanced Performance. *Nano-Micro Letters* **2016,** *9*, 19.
37. Kötz, R.; Carlen, M., Principles and applications of electrochemical capacitors. *Electrochimica Acta* **2000,** *45*, 2483.
38. Esfahani, M. Z.; Khosravi, M., Stamp-assisted flexible graphene-based micro-supercapacitors. *Journal of Power Sources* **2020,** *462*, 228166.
39. Li, J.; Sollami Delekta, S.; Zhang, P.; Yang, S.; Lohe, M. R.; Zhuang, X.; Feng, X.; Östling, M., Scalable Fabrication and Integration of Graphene Microsupercapacitors through Full Inkjet Printing. *ACS Nano* **2017,** *11*, 8249.
40. Sollami Delekta, S.; Adolfsson, K. H.; Benyahia Erdal, N.; Hakkarainen, M.; Östling, M.; Li, J., Fully inkjet printed ultrathin microsupercapacitors based on graphene electrodes and a nano-graphene oxide electrolyte. *Nanoscale* **2019,** *11*, 10172.
41. Wang, Y.; Zhang, Y.; Wang, G.; Shi, X.; Qiao, Y.; Liu, J.; Liu, H.; Ganesh, A.; Li, L., Direct Graphene-Carbon Nanotube Composite Ink Writing All-Solid-State Flexible Microsupercapacitors with High Areal Energy Density. *Advanced Functional Materials* **2020,** *30*, 1907284.
42. Ma, J.; Zheng, S.; Cao, Y.; Zhu, Y.; Das, P.; Wang, H.; Liu, Y.; Wang, J.; Chi, L.; Liu, S.; Wu, Z.-S., Aqueous MXene/PH1000 Hybrid Inks for Inkjet-Printing Micro-Supercapacitors with Unprecedented Volumetric Capacitance and Modular Self-Powered Microelectronics. *Advanced Energy Materials* **2021,** *11*, 2100746.
43. Bizet, K.; Gabrielli, C.; Perrot, H., Immunodetection by quartz crystal microbalance - A new approach for direct detection of rabbit IgG and peroxidase. *Applied Biochemistry and Biotechnology* **2000,** *89*, 139.
44. Gabrielli, C.; Garcia-Jareno, J. J.; Keddam, M.; Perrot, H.; Vicente, F., Ac-electrogravimetry study of electroactive thin films. I. Application to Prussian Blue. *Journal of Physical Chemistry B* **2002,** *106*, 3182.

Graphical Table of Contents

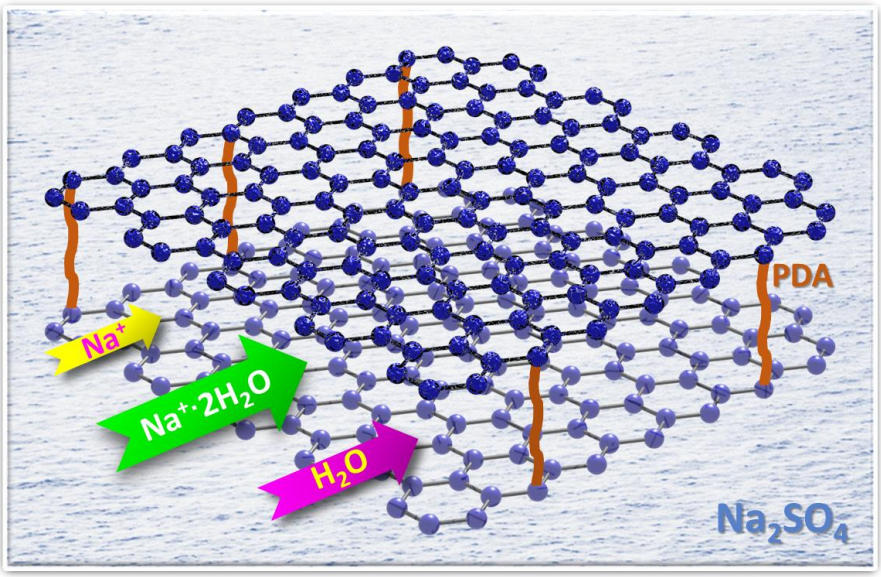


A 2D symmetrical all-solid micro-supercapacitor having high performances (energy density, cycling stability) is obtained using electrochemical reduced graphene oxide – polydopamine composite electrodes and a $Na_2SO_4$/PVA gel. The inorganic/organic composite electrode is first characterized in an aqueous electrolyte by *ac*-electrogravimetry that indicates the species involved in the charge storage processes ($Na^+ \cdot 2HO_2$, $Na^+$ and $H_2O$) and their transfer kinetics.